Available online at www.sciencedirect.com
SCIENCE DIRECT®
ELSEVIER
International Journal of Solids and Structures 42 (2005) 6433–6456
INTERNATIONAL JOURNAL OF SOLIDS and STRUCTURES
www.elsevier.com/locate/ijsolstr

Analytical solutions for single- and multi-span functionally graded plates in cylindrical bending

Z.G. Bian [a], W.Q. Chen [a,b,*], C.W. Lim [c], N. Zhang [d]

[a] *Department of Civil Engineering, Zhejiang University, Hangzhou 310027, PR China*
[b] *State Key Lab of CAD and CG, Zhejiang University, Hangzhou 310027, PR China*
[c] *Department of Building and Construction, City University of Hong Kong, Tat Chee Avenue, Kowloon, Hong Kong, PR China*
[d] *School of Civil and Environmental Engineering, Nanyang Technological University, Singapore 639798, Singapore*

Received 19 July 2004; received in revised form 11 April 2005
Available online 8 June 2005

Abstract

A recently developed plate theory using the concept of shape function of the transverse coordinate parameter is extended to determine the stress distribution in an orthotropic functionally graded plate subjected to cylindrical bending. The transfer matrix method is presented to derive the shape function. The equations governing the plate deformation are then solved analytically using the transfer matrix method for arbitrary boundary conditions. For a simply supported functionally graded plate, a comparison of the present solution with the exact elasticity solution, the first- and third-order shear deformation plate theories is presented and discussed. It is demonstrated that the present method yields more accurate stresses than the first- and third-order shear deformation theories. The effect of boundary conditions and inhomogeneity of material on the displacements and stresses in functionally graded plates are investigated. A multi-span functionally graded plate with arbitrary boundary conditions is further considered to demonstrate the efficiency of the present method.

Keywords: Functionally graded plate; Cylindrical bending; Shape function; State-space method; Multi-span plate

1. Introduction

Functionally graded materials (FGMs) were first developed by a group of Japanese scientists to address the needs of aggressive environment of thermal shock (Rabin and Shiota, 1995). Now, the concept of FGM

* Corresponding author. Address: Department of Civil Engineering, Zhejiang University, Hangzhou 310027, PR China. Tel.: +86 571 87952284; fax: +86 571 87952165.
E-mail address: chenwq@ccea.zju.edu.cn (W.Q. Chen).

0020-7683/$ - see front matter © 2005 Elsevier Ltd. All rights reserved.
doi:10.1016/j.ijsolstr.2005.04.032

has been widely explored in various engineering applications including electron, chemistry, optics, biomedicine, etc. (Koizumi, 1997). FGMs are usually more superior to the conventional laminated materials because of no discernible internal seams or boundaries, and no internal stress peaks are caused when external loads is applied and thus failure from interfacial debonding or from stress concentration can be avoided (Wu et al., 1996; Li and Weng, 2002). On the macroscopic scale, FGMs are anisotropic, inhomogeneous and possess spatially continuous mechanical properties, which bring the conventional mechanics into a brand-new field.

Heretofore, kinds of approximate theories have been extended to investigate the mechanical behavior of functionally graded plates (FGPs). For example, Aboudi et al. (1995) took the microstructural and macrostructural effects into account and developed a new kind of higher-order shear deformation plate theory for FGMs. Praveen and Reddy (1998) investigated the response of FGPs making use of a plate finite element (FE) that accounts for the transverse shear strains, rotary inertia and moderately large rotations in the von Kármán sense. Employing the first-order shear deformation Mindlin plate theory, Reddy et al. (1999) studied the axisymmetric bending and stretching of functionally graded solid and annular circular plates. On the basis of a higher-order shear deformation plate theory, Reddy (2000) further developed FE formulations for thick FGPs and studied the nonlinear dynamic response of FGPs subjected to a suddenly applied uniform pressure. Reddy's third-order shear deformation plate theory was also employed by Cheng and Batra (2000) to study the buckling and steady state vibrations of a simply supported isotropic polygonal FGP, and a correspondence between eigenvalues of such plates and those of membranes is established. Associating a second-order shear deformation plate theory with a laminated model, Liu et al. (2003) analyzed the dispersion of waves and characteristic wave surfaces in functionally graded piezoelectric plates with a FE method. Based on Reissner–Mindlin plate theory, Croce and Venini (2004) conducted a static analysis of rectangular FGPs using FE method. The FE method was recently used by Liew et al. (2004) to optimize the shape control of functionally graded smart plates by introducing a stochastic zeroth-order optimization algorithm. Based on the first-order shear deformation plate theory, Wu (2004) studied the thermal buckling of a simply supported moderately thick rectangular FGP. Qian et al. (2004) incorporated a higher-order shear and normal deformable plate theory with a meshless local Petrov–Galerkin method to analyze the static deformation and free or forced vibration of a thick rectangular FGP. More recently, Ma and Wang (2004) studied the axisymmetric bending and buckling problems of circular FGPs, and presented the relationships between solutions based on the classical plate theory and those based on a third-order shear deformation plate theory.

As is known to all, the classical plate and shell theories can be used to analyze thin plates and shells. For example, based on Love's shell theory, Lam and Li (1997) and Li and Lam (2001) investigated the free vibrations of rotating thin truncated circular homogeneous and laminated conical shells. Such theories, however, will produce unsatisfactory results in case of a low length-to-thickness ratio or a high ratio of elastic modulus to shear modulus, owing to the neglect of transverse shear deformation. For laminated plates and shells, even higher-order theories cannot give satisfactory stress estimation. A generalized refined theory was recently suggested by Soldatos and Watson (1997a,b) and Soldatos and Liu (2001), into which shape functions were incorporated to make sure that the calculated transverse shear stresses are continuous across the interfaces. The accuracy of this new theory in predicting stress distributions was demonstrated through numerical comparison.

In this paper, the above-mentioned plate theory (referred to as Soldatos plate theory hereafter) is extended to investigate the cylindrical bending behavior of FGPs. A laminate model is employed to approximate the FGP by assuming material homogeneity within each thin layer (Chen and Ding, 2000; Chen et al., 2003). Shall the method of Soldatos and Watson (1997a,b) and Soldatos and Liu (2001) to determine the shape function be employed, a total of $2N$ simultaneous equations (N is the layer number of the approximate laminate model of FGP) needs to be solved. Hence, it becomes very time-consuming when the number of divided layers increases. To overcome this difficulty, the shape function is derived by using the transfer matrix method (TMM), which was originally proposed by Thomson (1950) and followed by many

others (Haskell, 1953; Pestel and Leckie, 1963; Munjal, 1975, 1993; Folds and Loggins, 1977; Stepanishen and Strozeski, 1982; Nayfeh, 1991). A detailed description of the analysis procedure can be found in Khdeir (1996). The superiority of TMM is very obvious, for example, in the present determination of shape function, it allows us to always solve only a system of two equations regardless of how many layers are involved. The governing equations in Soldatos plate theory are also solved within the framework of TMM. For simply supported boundary conditions, a comparison of the present solution is made with the exact elasticity solution and the solutions obtained from the first- and third-order shear deformation plate theories. Numerical examples are presented to show the effect of boundary conditions and material inhomogeneity on the elastic field in functionally graded plates.

The final focus of the present paper is in the investigation of deformation of multi-span FGPs. Multi-span plates are frequently encountered in many engineering fields and thus it is important to understand their responses under various loading conditions. Generally, multi-span plates can be treated as plates with internal line supports (Zhou, 1994; Kong and Cheung, 1995). Cheung and Zhou (2000) used Rayleigh-Ritz method with a set of static beam functions to analyze the vibrations of orthotropic rectangular plates with elastic intermediate line-supports. Li (2003) applied an exact approach to determine the natural frequencies and mode shapes of a rectangular plate with a line concentrated mass and a line-spring support or with a line-spring-mass system. Xiang et al. (2002a,b) developed a Levy-type solution method to study the vibration of multi-span rectangular plates. In their analysis, the governing partial differential equation was first transformed into an ordinary differential equation by assuming a sinusoidal variation along the direction with two simply supported edges and then the ordinary differential equation was written in the form of a system of simultaneous equations of first-order, of which the solution could be easily obtained. Their procedure is very similar to TMM employed here. In the open literatures, however, few studies addressed the static deformation of multi-span plates, although it is of immense value to designers. In this paper, the TMM is further extended to obtain the analytical deformation solution of a multi-span FGP with arbitrary boundary conditions. Although TMM can be readily used to analyze plates with any number of spans, a three-span FGP is chosen as a numerical example to investigate the distributions of displacements and stresses in the span direction.

2. Basic equations for cylindrical bending

Consider an orthotropic FGP with an infinite extent in y-direction, as shown in Fig. 1. The plate is in a state of cylindrical bending so that only two displacements U and W, in x- and z-directions respectively, are nonzero and both are independent of the coordinate y. The thickness and length in x-direction are denoted as h and L respectively. We assume that the plate is arbitrarily inhomogeneous in the thickness direction, i.e. all elastic constants c_{ij} are arbitrary functions of z.

According to Soldatos and Watson (1997a), the displacement field can be taken as:

$$\begin{aligned} \overline{W}(\xi,\zeta) &= \bar{w}(\xi) \\ \overline{U}(\xi,\zeta) &= \bar{u}(\xi) - \zeta\frac{\mathrm{d}\bar{w}(\xi)}{\mathrm{d}\xi} + \bar{\varphi}_x(\zeta)\theta_x(\xi) \end{aligned} \tag{1}$$

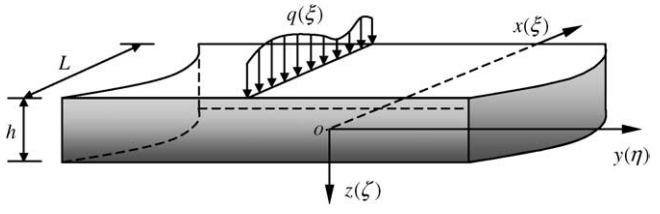

Fig. 1. Cartesian coordinates and plate geometry.

where $\xi = x/h$, $\zeta = z/h$, and $\bar{\Theta} = \Theta/h$, here Θ represents any one of U, W, u, w and φ_x. Obviously, $\bar{u}$ and $\bar{w}$ are dimensionless displacements in the middle plane $\zeta = 0$, and θ_x denotes the transverse shear strain in the same plane. $\bar{\varphi}_x$ is the dimensionless shape function to be determined. To make the displacement field in Eq. (1) physically meaningful, it is assumed that (Soldatos and Watson, 1997a)

$$\bar{\varphi}_x|_{\zeta=0} = 0, \quad \left.\frac{\mathrm{d}\bar{\varphi}_x}{\mathrm{d}\zeta}\right|_{\zeta=0} = 1 \tag{2}$$

It can be shown that the above Soldatos theory degenerates to the classical plate theory, the first- and third-order shear deformation plate theories, by assuming $\bar{\varphi}_x = 0$, ζ and $\zeta(1 - 4\zeta^2/3)$ respectively.

The strain field corresponding to Eq. (1) can be obtained as

$$\begin{aligned} &\varepsilon_{xx} = \frac{\mathrm{d}\bar{u}}{\mathrm{d}\xi} - \zeta\frac{\mathrm{d}^2\bar{w}}{\mathrm{d}\xi^2} + \bar{\varphi}_x\frac{\mathrm{d}\theta_x}{\mathrm{d}\xi}, \quad \varepsilon_{zx} = \theta_x\frac{\mathrm{d}\bar{\varphi}_x}{\mathrm{d}\zeta} \\ &\varepsilon_{yy} = \varepsilon_{zz} = \varepsilon_{xy} = \varepsilon_{yz} = 0 \end{aligned} \tag{3}$$

For an orthotropic FGP, the generalized constitutive relations are:

$$\begin{aligned} &\bar{\sigma}_{xx} = \left(\bar{c}_{11} - \frac{\bar{c}_{13}^2}{\bar{c}_{33}}\right)\varepsilon_{xx} = \alpha_1\varepsilon_{xx} \\ &\bar{\sigma}_{yy} = \left(\bar{c}_{12} - \frac{\bar{c}_{13}\bar{c}_{23}}{\bar{c}_{33}}\right)\varepsilon_{xx} = \alpha_2\varepsilon_{xx} \\ &\bar{\sigma}_{zx} = \bar{c}_{66}\varepsilon_{zx} = \alpha_3\varepsilon_{zx} \end{aligned} \tag{4}$$

where $\bar{\sigma}_{ij} = \sigma_{ij}/c_{44}^b$ and $\bar{c}_{ij} = c_{ij}/c_{44}^b$, in which c_{44}^b is the elastic constant on the bottom surface ($\zeta = 0.5$).

Consider the FGP subject to a normal and downward load $q(\xi)$ on its top surface, as shown in Fig. 1. In light of the principle of the minimum potential energy, the equations of equilibrium can be derived as:

$$\frac{\mathrm{d}N_x}{\mathrm{d}\xi} = 0, \quad \frac{\mathrm{d}^2M_x}{\mathrm{d}\xi^2} = -\frac{q}{c_{44}^b}, \quad \frac{\mathrm{d}M_x^a}{\mathrm{d}\xi} = Q_x \tag{5}$$

where the generalized resultant forces are defined by

$$N_x = \int_{-0.5}^{0.5}\bar{\sigma}_{xx}\,\mathrm{d}\zeta, \quad Q_x = \int_{-0.5}^{0.5}\frac{\mathrm{d}\bar{\varphi}_x}{\mathrm{d}\zeta}\bar{\sigma}_{zx}\,\mathrm{d}\zeta, \quad M_x = \int_{-0.5}^{0.5}\bar{\sigma}_{xx}\zeta\,\mathrm{d}\zeta, \quad M_x^a = \int_{-0.5}^{0.5}\bar{\varphi}_x\bar{\sigma}_{xx}\,\mathrm{d}\zeta \tag{6}$$

Meanwhile, the boundary conditions at $\xi = 0$ and $\xi = a = L/h$ are

$$\begin{aligned} &N_x = 0 \text{ or } \bar{u} \text{ prescribed}; \quad M_x^a = 0 \text{ or } \theta_x \text{ prescribed} \\ &\frac{\mathrm{d}M_x}{\mathrm{d}\xi} = 0 \text{ or } \bar{w} \text{ prescribed}; \quad M_x = 0 \text{ or } \frac{\mathrm{d}\bar{w}}{\mathrm{d}\xi} = 0 \text{ prescribed} \end{aligned} \tag{7}$$

Three typical boundary conditions are as follows:

$$\begin{aligned} &\text{Simply supported(S):} \quad N_x = M_x^a = \bar{w} = M_x = 0 \\ &\text{Free(F):} \quad N_x = M_x^a = \frac{\mathrm{d}M_x}{\mathrm{d}\xi} = M_x = 0 \\ &\text{Clamped(C):} \quad \bar{u} = \theta_x = \bar{w} = \frac{\mathrm{d}\bar{w}}{\mathrm{d}\xi} = 0 \end{aligned} \tag{8}$$

3. Determination of the shape function

A proper shape function plays a significant role in improving the accuracy of the stress analysis. In Soldatos plate theory, the shape function $\bar{\varphi}_x$ is derived from the following three-dimensional equation of equilibrium

$$\frac{\partial \bar{\sigma}_{xx}}{\partial \xi} + \frac{\partial \bar{\sigma}_{xz}}{\partial \zeta} = 0 \tag{9}$$

Since the plate under consideration is inhomogeneous along the thickness, it is very difficult to deal with such a case directly, except for some particular circumstances. Here, an approximate laminate model is employed. In this model, the FGP is evenly divided into $2N$ thin layers, so that each layer can be regarded as a homogeneous layer. In the following analysis, the material constants of each layer are assumed to take the corresponding values at the mid-plane of that layer.

In view of Eqs. (3), (4) and (9), one can obtain the following equation within the ith layer

$$\alpha_3^{(i)} \frac{\mathrm{d}^2 \bar{\varphi}_x^{(i)}}{\mathrm{d}\zeta^2} \theta_x = -\alpha_1^{(i)} \left[\bar{\varphi}_x^{(i)} \frac{\mathrm{d}^2 \theta_x}{\mathrm{d}\xi^2} - \frac{\mathrm{d}^3 \bar{w}}{\mathrm{d}\xi^3} \zeta + \frac{\mathrm{d}^2 \bar{u}}{\mathrm{d}\xi^2} \right] \tag{10}$$

where the superscript (i) corresponds to the ith layer of the laminate model. The special solution of Eq. (10) can be taken as (Soldatos and Watson, 1997a)

$$\bar{u} = A' \cos(\beta\xi), \quad \bar{w} = B' \sin(\beta\xi), \quad \theta_x = C' \cos(\beta\xi) \tag{11}$$

where $\beta = \pi/a$.

According to the treatment in Soldatos and Watson (1997a), the number of equations to be solved ultimately increases with increasing number of layers. Thus, if the material property of FGP varies distinctly along the thickness direction, for which a large number of layers are necessary to assure accuracy of the laminate model, the determination of shape function will be very time-consuming. In the following, we will adopt TMM to improve the efficiency of analysis.

Substituting Eq. (11) into Eq. (10) and rearranging the equations yield a system of first-order equations

$$\frac{\mathrm{d}}{\mathrm{d}\zeta} \mathbf{X}_i = \mathbf{T}_i \mathbf{X}_i - B\beta\zeta \mathbf{P}_i + A\mathbf{P}_i \tag{12}$$

where $\mathbf{X}_i = [\bar{\varphi}_x^{(i)}, \bar{\phi}_x^{(i)}]^{\mathrm{T}}$, $\bar{\phi}_x^{(i)} = \alpha_3^{(i)} \mathrm{d}\bar{\varphi}_x^{(i)}/\mathrm{d}\zeta$, $A = A'/C'$, $B = B'/C'$, and

$$\mathbf{T}_i = \begin{bmatrix} 0 & 1/\alpha_3^{(i)} \\ \beta^2 \alpha_1^{(i)} & 0 \end{bmatrix}, \quad \mathbf{P}_i = \begin{Bmatrix} 0 \\ \beta^2 \alpha_1^{(i)} \end{Bmatrix} \tag{13}$$

The solution to Eq. (12) is (Pestel and Leckie, 1963):

$$\begin{aligned} \mathbf{X}_i(\zeta) = {} & \exp[\mathbf{T}_i(\zeta - \zeta_{i,0})] \cdot \mathbf{X}_i(\zeta_{i,0}) - B \left\{ \int_{\zeta_{i,0}}^{\zeta} \exp[\mathbf{T}_i(\zeta - \tau)] \beta\tau \, \mathrm{d}\tau \right\} \mathbf{P}_i \\ & + A \left\{ \int_{\zeta_{i,0}}^{\zeta} \exp[\mathbf{T}_i(\zeta - \tau)] \, \mathrm{d}\tau \right\} \mathbf{P}_i, \quad (\zeta_{i,0} \leqslant \zeta \leqslant \zeta_{i,1}) \end{aligned} \tag{14}$$

where $\zeta_{i,0} = (i-1)/(2N) - 0.5$ and $\zeta_{i,1} = i/(2N) - 0.5$.

The continuity of displacement U and shear stress σ_{zx} at each fictitious interface requires $\bar{\varphi}_x$ and $\bar{\phi}_x$ be continuous there, which in turn yields

$$\mathbf{X}_i(\zeta_{i,1}) = \mathbf{H}_{i,j} \mathbf{X}_j(\zeta_{j,0}) - B\mathbf{K}_{i,j} + A\mathbf{J}_{i,j} \quad (i \geqslant j) \tag{15}$$

where the 2×2 matrices $\mathbf{H}_{i,j}$, $\mathbf{K}_{i,j}$, and $\mathbf{J}_{i,j}$ are defined by

$$\begin{aligned}\mathbf{H}_{i,j} &= \prod_{k=i}^{j} \exp\left(\frac{\mathbf{T}_k}{2N}\right)\\ \mathbf{K}_{i,j} &= \sum_{k=i}^{j}\left\{\mathbf{H}_{i,k+1}\cdot\int_{\zeta_{k,0}}^{\zeta_{k,1}} \exp[\mathbf{T}_k(\zeta_{k,1}-\zeta)]\beta\zeta\,\mathrm{d}\zeta\cdot\mathbf{P}_k\right\}\\ \mathbf{J}_{i,j} &= \sum_{k=i}^{j}\left\{\mathbf{H}_{i,k+1}\cdot\int_{\zeta_{k,0}}^{\zeta_{k,1}} \exp[\mathbf{T}_k(\zeta_{k,1}-\zeta)]\,\mathrm{d}\zeta\cdot\mathbf{P}_k\right\}\end{aligned} \tag{16}$$

The boundary condition $\bar{\sigma}_{zx}\big|_{\zeta=\pm 0.5}=0$ is equivalent to $\bar{\phi}_x\big|_{\zeta=\pm 0.5}=0$. Combining it with Eq. (2) yields

$$\begin{bmatrix} H^{11}_{N,1} & -K^{1}_{N,1} & J^{1}_{N,1}\\ H^{21}_{N,1} & -K^{2}_{N,1} & J^{2}_{N,1}\\ 0 & K^{2}_{2N,N+1} & -J^{2}_{2N,N+1}\end{bmatrix}\begin{Bmatrix}\bar{\varphi}^{(1)}_x(-0.5)\\ B\\ A\end{Bmatrix}=\alpha_3^{(N)}\begin{Bmatrix}0\\1\\H^{22}_{2N,N+1}\end{Bmatrix} \tag{17}$$

where $H^{ij}_{k,l}$, $K^{i}_{k,l}$, and $J^{i}_{k,l}$ denote the elements of the matrices $\mathbf{H}_{k,l}$, $\mathbf{K}_{k,l}$ and $\mathbf{J}_{k,l}$, respectively. From Eq. (17), the value of shape function at the top surface is determined and those at any other position can then be evaluated from Eq. (14).

4. FGP in cylindrical bending

The transfer matrix method described in the previous section is also employed to solve the governing equations of Soldatos plate theory. First, we rewrite Eqs. (3)–(6) in the following form:

$$\mathbf{D}\frac{\mathrm{d}\mathbf{V}}{\mathrm{d}\xi}=\mathbf{Z}\mathbf{V}+\mathbf{S} \tag{18}$$

where $\mathbf{V}=[\bar{u}\ \bar{w}\ \theta_x\ \Gamma_w\ N_x\ T\ M_x^a\ M_x]^{\mathrm{T}}$ and $\mathbf{S}=(q/c_{44}^b)[\bar{q}_0+\bar{q}_1\ \mathbf{0}_{1\times 7}]^{\mathrm{T}}$, in which $\Gamma_w=\mathrm{d}\bar{w}/\mathrm{d}\xi$ and $T=\mathrm{d}M_x/\mathrm{d}\xi$. The expressions for matrices $\mathbf{D}$ and $\mathbf{Z}$ are given in Appendix A.

The solution to Eq. (18) is

$$\mathbf{V}(\xi)=\exp(\xi\mathbf{D}^{-1}\mathbf{Z})\cdot\mathbf{V}(0)-\int_0^{\xi}\exp[(\xi-\tau)\mathbf{D}^{-1}\mathbf{Z}]\cdot\mathbf{D}^{-1}\mathbf{S}(\tau)\,\mathrm{d}\tau \tag{19}$$

Setting $\xi=a$ in Eq. (19) establishes a relationship between the vector $\mathbf{V}$ at $\xi=0$ and $\xi=a$. Imposing the boundary conditions in Eq. (8) leads to a set of solvable algebraic equations, from which one can determine $\mathbf{V}(0)$ for the three typical boundary conditions. The vector at any position, $\mathbf{V}(\xi)$, is then calculated according to Eq. (19). The stress field is obtained ultimately by the virtual of Eqs. (3) and (4).

5. Multi-span FGP

Finally we investigate an FGP of multiple spans along the x-direction, as shown in Fig. 2. For a multi-span FGP, the shear force T is discontinuous at internal supports. Hence, we shall designate T_i^- and T_i^+ to the values of T at the left side and right side of the ith support. The vectors $\mathbf{V}_i^-$ and $\mathbf{V}_i^+$ are also introduced correspondingly.

Without loss of generality, we assume each span has the same length a. From Eq. (19), we obtain:

$$\mathbf{V}_i^-=\mathbf{L}\mathbf{V}_{i-1}^+ +\mathbf{R} \tag{20}$$

where $\mathbf{L}=\exp(a\mathbf{D}^{-1}\mathbf{Z})$, and $\mathbf{R}=\int_0^a \exp[(a-\tau)\mathbf{D}^{-1}\mathbf{Z}]\cdot\mathbf{D}^{-1}\mathbf{S}(\tau)\,\mathrm{d}\tau$.

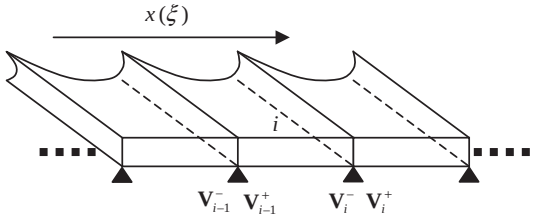

Fig. 2. Diagrammatic sketch of a multi-span FGP.

To implement the analysis, a new vector is introduced

$$\widetilde{\mathbf{V}} = [\,\bar{u} \quad \bar{w} \quad \theta_x \quad \Gamma_w \quad N_x \quad 0 \quad M_x^a \quad M_x\,]^{\mathrm{T}} \tag{21}$$

By making use of $\bar{w} = 0$ at internal supports, we obtain:

$$T_{i-1}^{+} = -\frac{1}{L_{26}}(\mathbf{L}_{r2}\widetilde{\mathbf{V}}_{i-1} - R_2) \quad (i = 1, 2, \ldots, n-1) \tag{22}$$

$$\widetilde{\mathbf{V}}_i = \widetilde{\mathbf{L}} \cdot \widetilde{\mathbf{V}}_{i-1} + \widetilde{\mathbf{R}} \quad (i = 1, 2, \ldots, n-1) \tag{23}$$

where L_{ij} and R_i are elements of the matrix $\mathbf{L}$ and the column $\mathbf{R}$ respectively, $\mathbf{L}_{r2}$ is a 1×8 row matrix consisting of the elements on the second row of matrix $\mathbf{L}$, and n is the number of span. The expressions for $\widetilde{\mathbf{L}}$ and $\widetilde{\mathbf{R}}$ are listed in Appendix A.

Combining Eq. (23) with Eq. (20), yields:

$$\mathbf{V}_n^{-} = (\mathbf{L} \cdot \breve{\mathbf{L}}_{n-1}) \cdot \widetilde{\mathbf{V}}_0 + \mathbf{L}_{c6} \cdot T_{n-1}^{+} + \mathbf{L} \cdot \breve{\mathbf{R}}_{n-1} + \mathbf{R} \tag{24}$$

where $\breve{\mathbf{L}}_{n-1} = (\widetilde{\mathbf{L}})^{n-1}$, $\breve{\mathbf{R}}_{n-1} = \left[\sum_{k=n-2}^{0}(\widetilde{\mathbf{L}})^{k}\right] \cdot \widetilde{\mathbf{R}}$, and $\mathbf{L}_{c6}$ is an 8×1 column matrix consisting of the elements on the sixth column of the matrix $\mathbf{L}$. Applying the boundary conditions in Eq. (8) into Eq. (24), leads to a system of algebraic equations that completely determines $\widetilde{\mathbf{V}}_0$ and T_{n-1}^{+}. By the virtue of Eqs. (22) and (23), $\widetilde{\mathbf{V}}_i$ and T_i^{+} at each support can be obtained, from which we then have

$$\mathbf{V}_i^{+} = \widetilde{\mathbf{V}}_i + [\,0 \quad 0 \quad 0 \quad 0 \quad 0 \quad T_i^{+} \quad 0 \quad 0\,]^{\mathrm{T}} \tag{25}$$

Finally, $\mathbf{V}(\xi)$ in every span can be determined from Eq. (19).

6. Numerical examples

First, the present TMM formulations are verified by examining the numerical examples considered by Soldatos and Watson (1997a), for which identical results have been obtained. Second, although Soldatos and Watson (1997a,b) and Soldatos and Liu (2001) have made meaningful comparisons between Soldatos plate theory and the elasticity solution methods, here calculation is presented for a two-layered plate subjected to a uniformly distributed lateral load (Vel and Batra, 2001). The material and geometric properties can be found in Vel and Batra (2000). As we can see from Table 1, the present results are very satisfactory as compared with the elasticity solution, denoted as VB in the table, in Vel and Batra (2001), who employed the Eshelby–Stroh formalism (Vel and Batra, 2000).

Next, we investigate the deformation of single-span FGPs. In the following numerical examples, a mechanical loading $q = q_1 \sin(\beta\xi)$ applied on the top surface is considered. As regards the distribution of

Table 1
Comparison of a two-layered plate subjected to various boundary conditions

$L/h = 4$	C–C		C–F (cantilever)		C–S	
	VB	Present	VB	Present	VB	Present
$100E_T h^2 U(0.75a, -0.5)/(q_1 L^3)$	−2.283	−2.537	32.453	31.670	−4.702	−4.634
$100E_T h^3 W(0.5a, 0)/(q_1 L^4)$	3.212	2.939	19.132	18.550	4.257	4.089
$h^2\sigma_{xx}(0.5a, -0.5)/(q_1 L^2)$	−0.131	−0.121	0.189	0.190	−0.191	−0.180
$h^2\sigma_{xx}(0.75a, 0.5)/(q_1 L^2)$	0.341	0.359	−0.353	−0.354	1.336	1.349
$h\sigma_{zx}(0.25a, 0.25)/(q_1 L)$	0.509	0.547	1.589	1.644	0.717	0.776
$h\sigma_{zx}(0.75a, 0.25)/(q_1 L)$	−0.509	−0.547	0.602	0.549	−0.332	−0.320
$\sigma_{zz}(0.5a, -0.25)/q_1$	−0.938	−0.939	−0.935	−0.939	−0.940	−0.939

material properties, there are several models in literature (Delale and Erdogan, 1988; Fuchiyama and Noda, 1995; Liu et al., 1999; Chen et al., 2002). Here we consider the following typical model (Chen et al., 2004a):

$$\Psi = \Psi^0(\Psi^1/\Psi^0)^\gamma \tag{26}$$

where $\gamma = (\zeta + 0.5)^\kappa$, Ψ represents an arbitrary material constant of FGM, while Ψ^0 and Ψ^1 are the corresponding ones for two homogeneous materials. The material constants of the two homogeneous materials considered in this paper are listed in Table 2. Fig. 3 shows the variations of the elastic constant c_{11} along the thickness direction for several values of κ.

The through-thickness distribution of shape function $\bar{\varphi}_x$ is demonstrated in Fig. 4. Different from the conventional first- and third-order shear deformation plate theories, in which the transverse shear deforma-

Table 2
Material constants of two homogenous materials (units: 10^{10} N/m^2)

Property	c_{11}	c_{12}	c_{13}	c_{22}	c_{23}	c_{33}	c_{44}	c_{55}	c_{66}
Ψ^0	40.17	0.33	0.34	1.07	0.27	1.07	0.50	0.70	0.50
Ψ^1	15.98	0.47	0.47	1.20	1.20	1.20	0.55	0.42	0.42

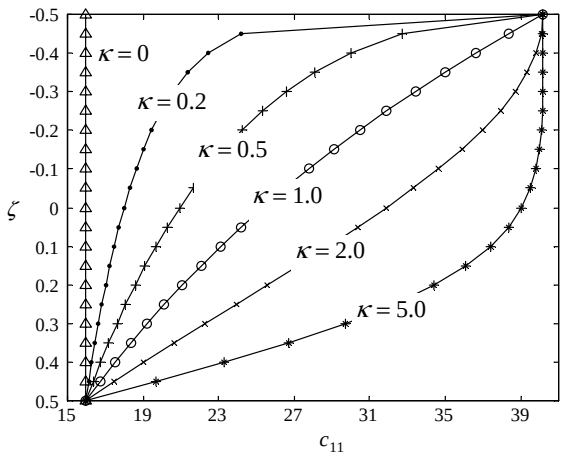

Fig. 3. Variation of elastic constant c_{11} through thickness.

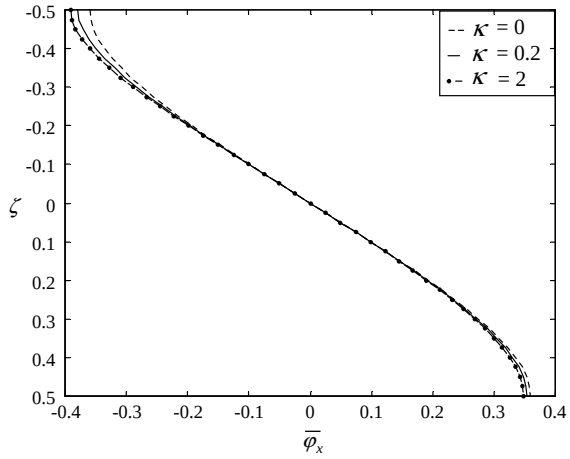

Fig. 4. Variation of shape function $\bar{\varphi}_x$ through thickness.

tion remains invariant once the displacement field is assumed, the shape function in Soldatos plate theory changes with κ. This self-adjustable property makes Soldatos plate theory more suitable for analyzing FGPs.

Figs. 5–10 illustrate a comparison of numerical solutions among the present method, the exact elasticity theory, the first- and third-order shear deformation plate theories. The exact results are obtained by a state-space method, which is outlined in Appendix B for the readers' convenience. The parameter κ in the material model, Eq. (26), is assigned 0.5, and only simply-supported conditions are considered in these numerical examples.

The through-thickness distributions of transverse displacement $\bar{w}$, normal stress $\bar{\sigma}_{xx}$ and shear stress $\bar{\sigma}_{zx}$ are shown in Figs. 5–7 respectively. The length-to-thickness ratio is taken as $L/h = 6$. Since all the simplified theories considered here (Soldatos plate theory, the first- and the third-order shear deformation plate theories) do not have transverse displacement $\bar{w}$ varying with the thickness coordinate, the results of the simplified theories are somewhat different from the actual situation as predicted from the exact elasticity

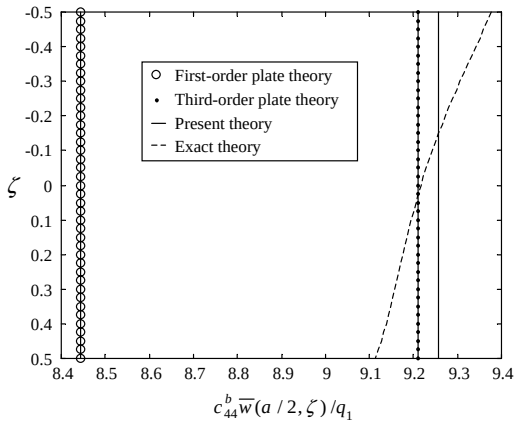

Fig. 5. Distribution of transverse displacement predicted by different theories ($L/h = 6$).

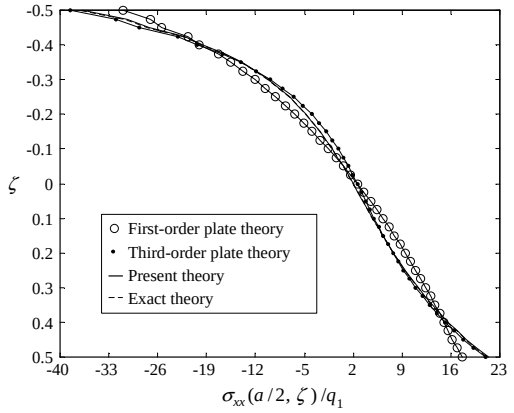

Fig. 6. Distribution of normal stress predicted by different theories ($L/h = 6$).

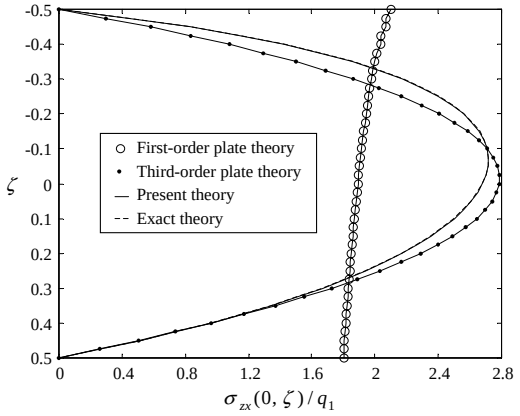

Fig. 7. Distribution of shear stress predicted by different theories ($L/h = 6$).

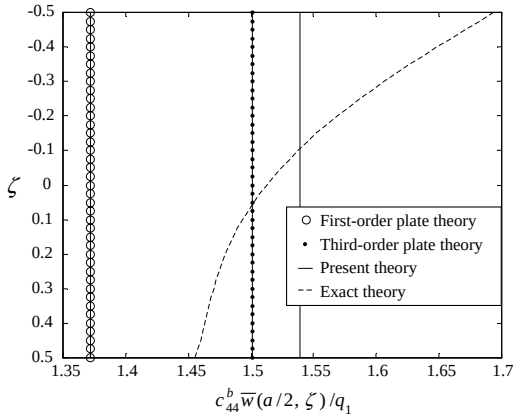

Fig. 8. Distribution of transverse displacement predicted by different theories ($L/h = 3$).

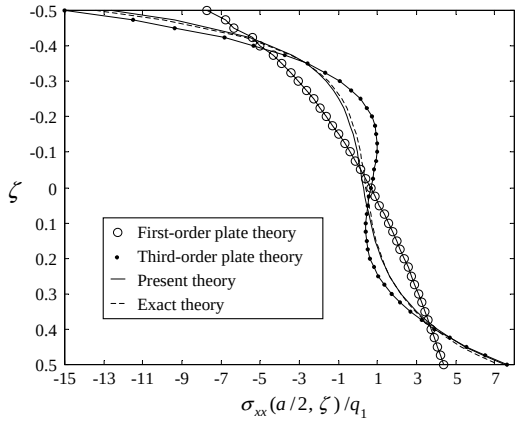

Fig. 9. Distribution of normal stress predicted by different theories ($L/h = 3$).

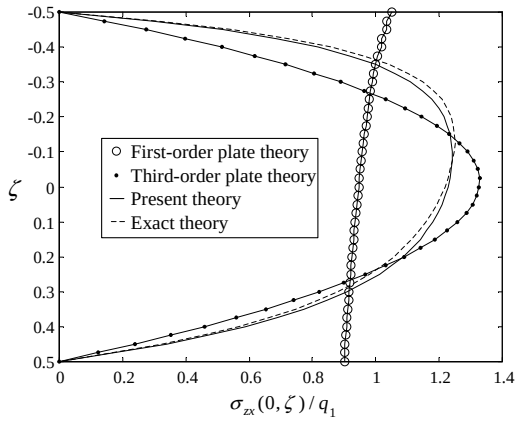

Fig. 10. Distribution of shear stress predicted by different theories ($L/h = 3$).

solution, as shown in Fig. 5. However, the transverse deflection obtained by the present method and that by the third-order shear deformation plate theory are almost identical, and both are close to the average value of that obtained by the exact solution. On the contrary, the first-order shear deformation plate theory underestimates the transverse deflection because the first-order shear deformable plate is generally stiffer than the actual plate due to the additional constraints assumed on deformation. Fig. 6 shows excellent agreement between the present solution and the exact solution. Such a conclusion is demonstrated explicitly in Fig. 7, where the first-order shear deformation plate theory only predicts the average value of the exact shear stress, and the peak position of shear stress predicted by the third-order shear deformation plate theory has an obvious departure from the exact one.

The results shown in Figs. 8–10 are for a smaller length-to-thickness ratio, i.e. $L/h = 3$. Similar conclusions can be reached except that the deviation of the third-order theory from the exact solution becomes a little more obvious. Thus, when compared to the first- and third-order shear deformation plate theories, the present method predicts the stress distribution more accurately if the plate is inhomogeneous or has a small length-to-thickness ratio.

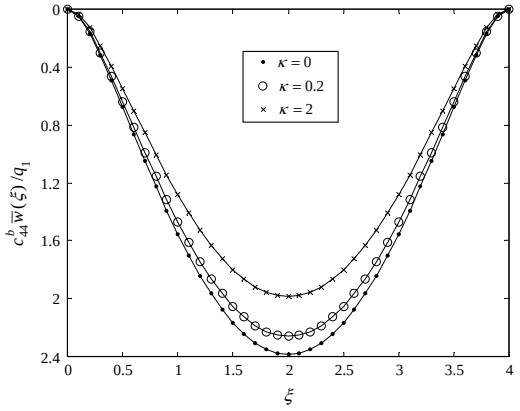

Fig. 11. Through-span distributions of deflection for different values of κ.

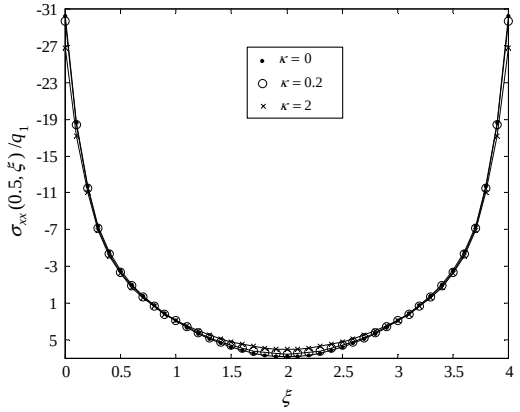

Fig. 12. Through-span distributions of normal stress for different values of κ.

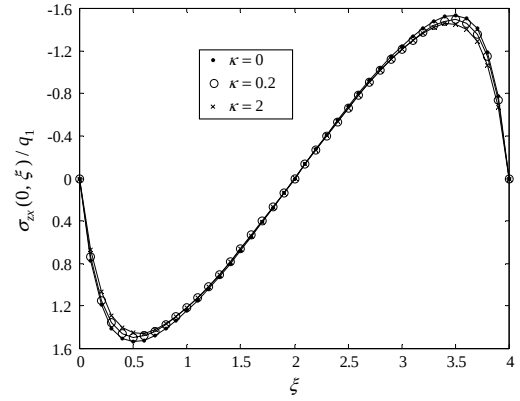

Fig. 13. Through-span distributions of shear stress for different values of κ.

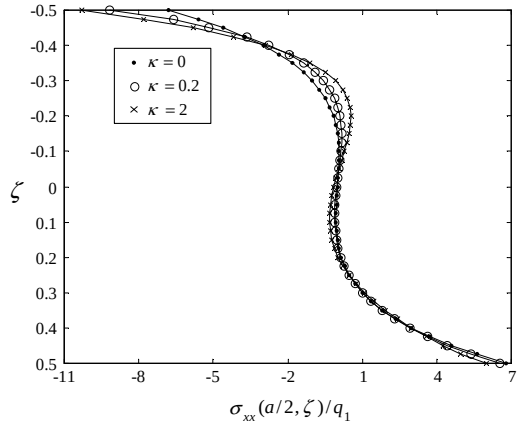

Fig. 14. Through-thickness distributions of normal stress for different values of κ.

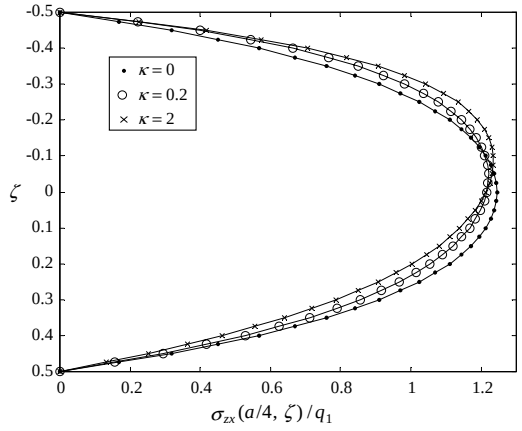

Fig. 15. Through-thickness distributions of normal stress for different values of κ.

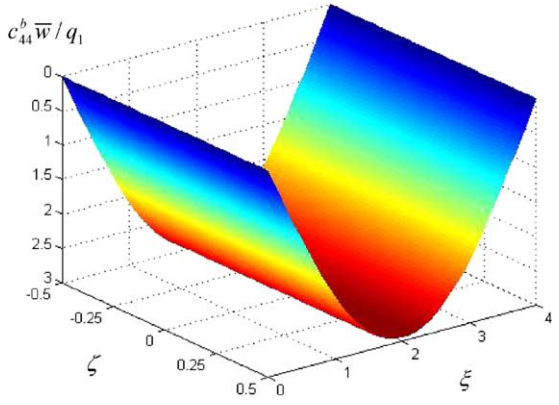

Fig. 16. Deflection of an FGP with SS boundary conditions.

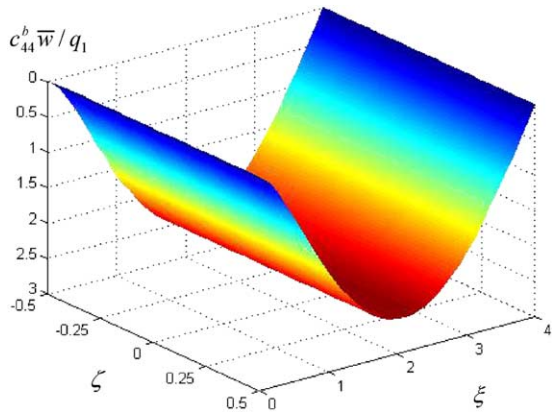

Fig. 17. Deflection of an FGP with CS boundary conditions.

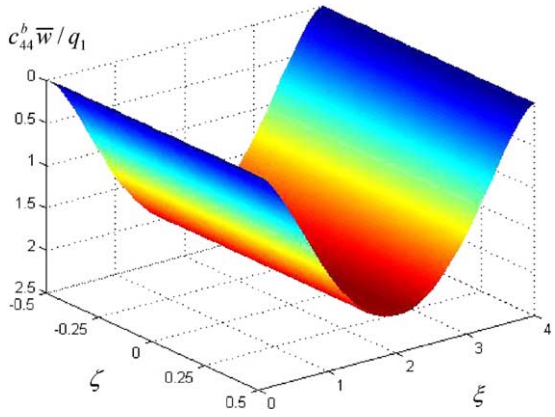

Fig. 18. Deflection of an FGP with CC boundary conditions.

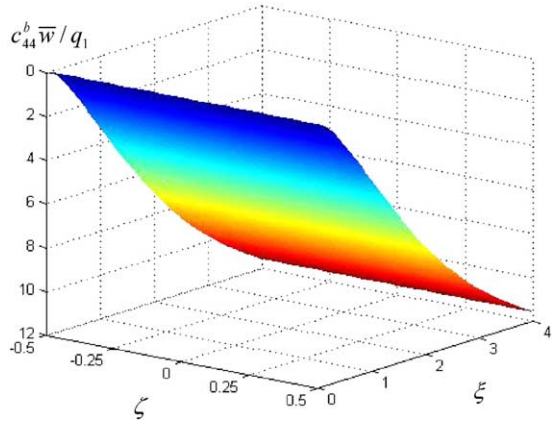

Fig. 19. Deflection of an FGP with CF boundary conditions.

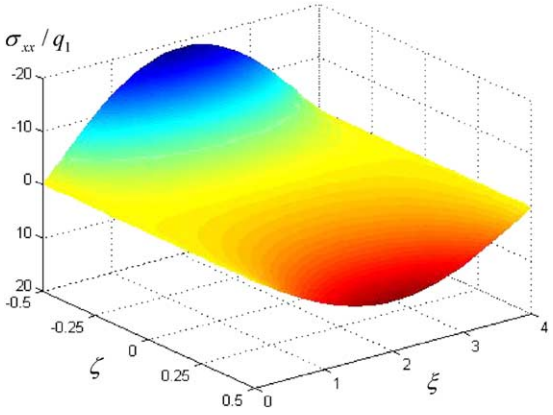

Fig. 20. Normal stress of an FGP with SS boundary conditions.

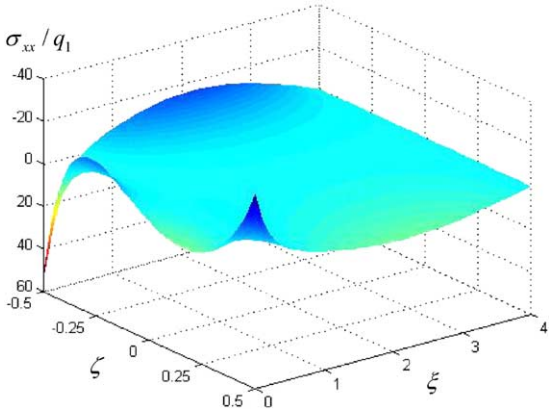

Fig. 21. Normal stress of an FGP with CS boundary conditions.

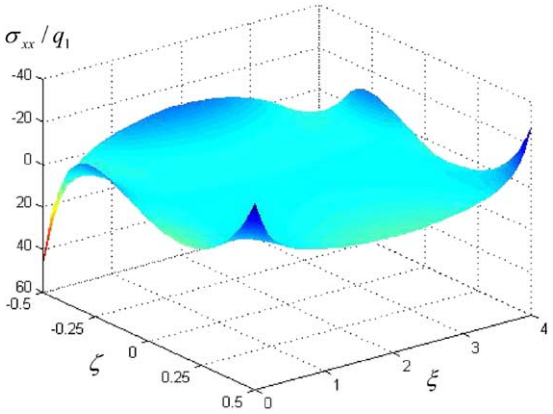

Fig. 22. Normal stress of an FGP with CC boundary conditions.

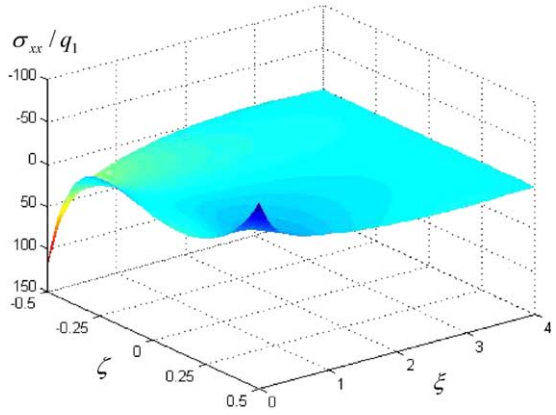

Fig. 23. Normal stress of an FGP with CF boundary conditions.

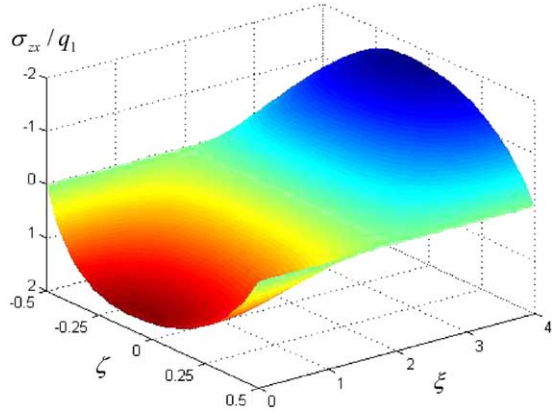

Fig. 24. Shear stress of an FGP with SS boundary conditions.

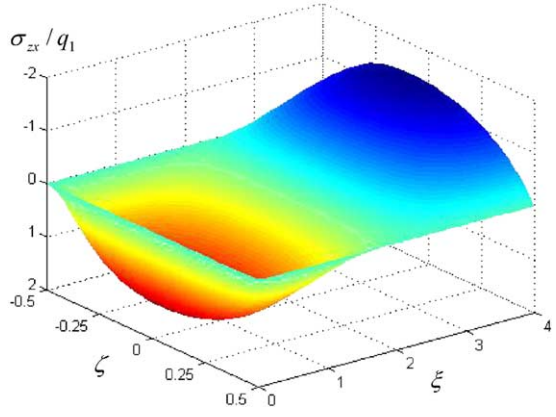

Fig. 25. Shear stress of an FGP with CS boundary conditions.

After checking the reliability, the present method is now applied to investigate the effect of κ on the distribution of displacements and stresses. Figs. 11–15 display the numerical results for different values of κ. In the calculation, $L/h = 4$ is taken and CC boundary condition is assumed. Several conclusions can be drawn from these figures. First, one can choose appropriate distribution of displacements and stresses for a practical engineering purpose by changing κ (the inhomogeneity parameter of FGM). Second, the effect of κ on deflection is more significant than that on stresses, and the effect of κ on the shear stress is more significant than that on normal stresses. Finally, positions of peak shear stresses in invariable with respect to κ, as shown in Fig. 15.

The effect of boundary conditions on displacements and stresses is studied and the results are shown spatially in Figs. 16–27, for which the length-to-thickness ratio is $L/h = 4$ and the inhomogeneity parameter is $\kappa = 1$.

Finally, the proposed analysis is employed to investigate the behavior of a three-span FGP with $\kappa = 1$. Each span is subjected to the same loading $q = q_1 \sin(\beta\xi)$ and the length-to-thickness ratio of each span plate is assumed as 4. The results are shown in Figs. 28–30.

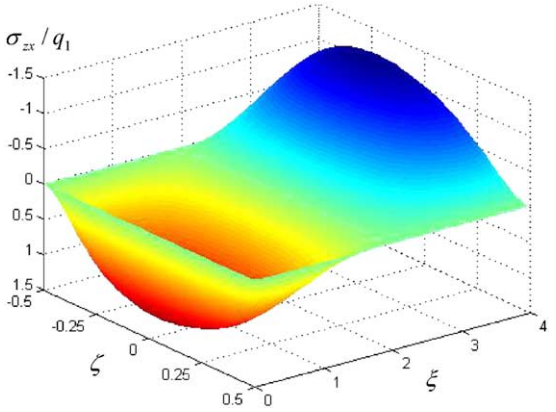

Fig. 26. Shear stress field of an FGP with CC boundary conditions.

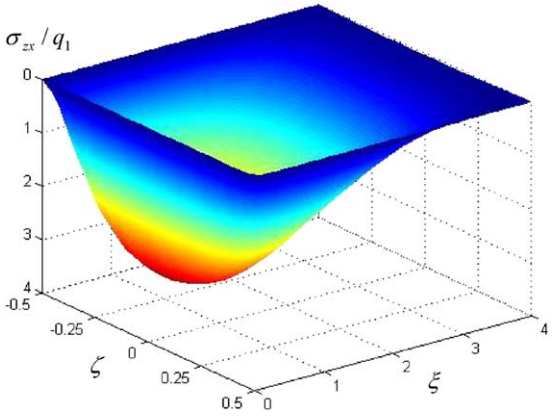

Fig. 27. Shear stress of an FGP with CF boundary conditions.

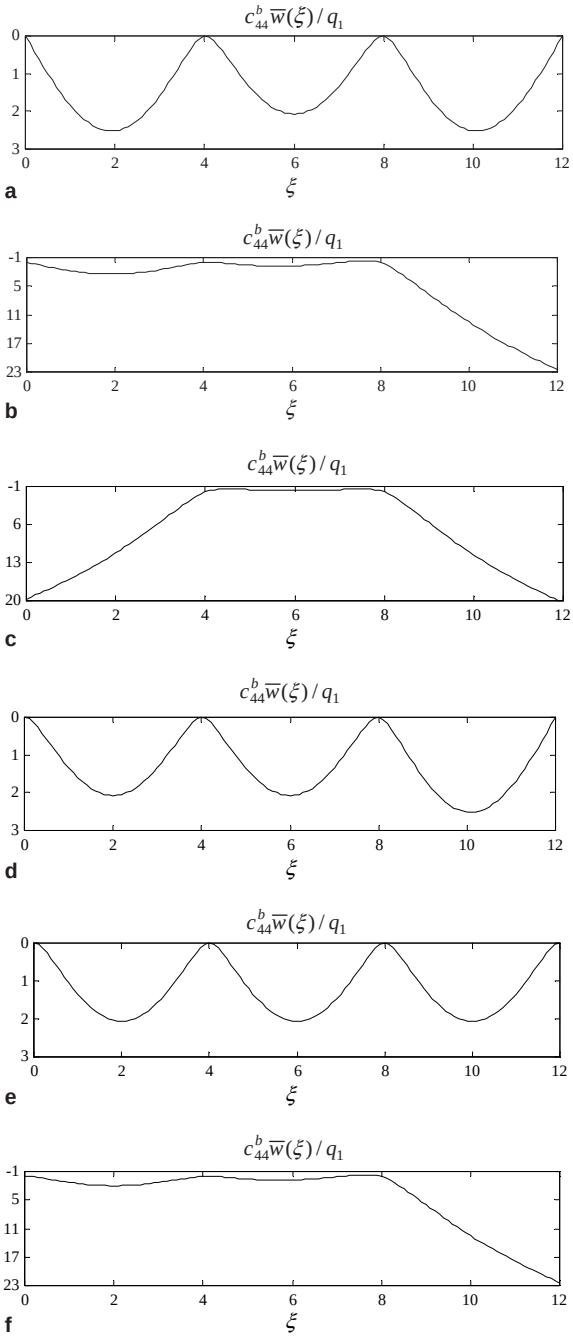

Fig. 28. (a) Distribution of deflection of a 3-span FGP with SS boundary conditions. (b) Distribution of deflection of a 3-span FGP with SF boundary conditions. (c) Distribution of deflection of a 3-span FGP with FF boundary conditions. (d) Distribution of deflection of a 3-span FGP with CS boundary conditions. (e) Distribution of deflection of a 3-span FGP with CC boundary conditions. (f) Distribution of deflection of a 3-span FGP with CF boundary conditions.

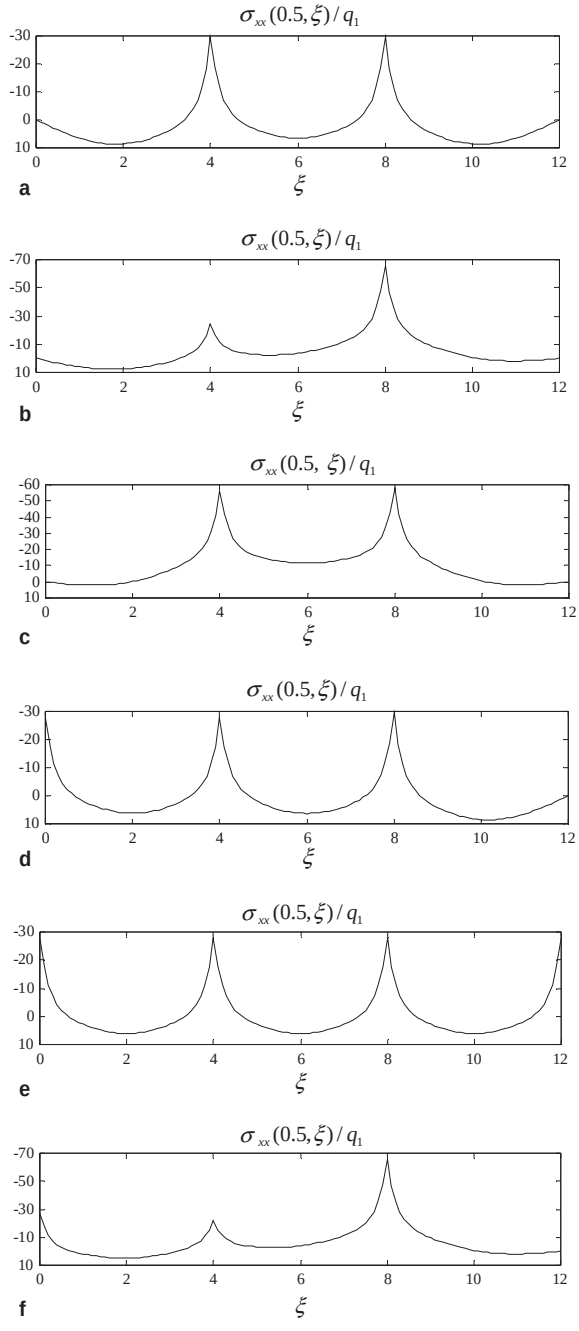

Fig. 29. (a) Distribution of normal stress of a 3-span FGP with SS boundary conditions. (b) Distribution of normal stress of a 3-span FGP with SF boundary conditions. (c) Distribution of normal stress of a 3-span FGP with FF boundary conditions. (d) Distribution of normal stress of a 3-span FGP with CS boundary conditions. (e) Distribution of normal stress of a 3-span FGP with CC boundary conditions. (f) Distribution of normal stress of a 3-span FGP with CF boundary conditions.

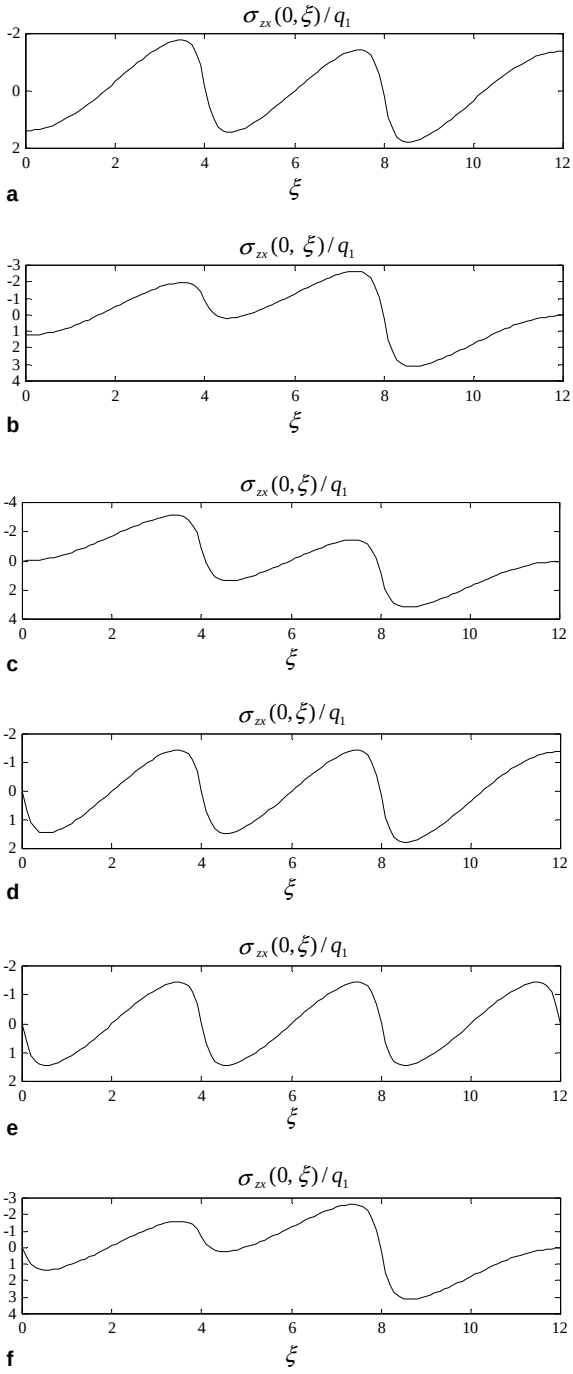

Fig. 30. (a) Distribution of shear stress of a 3-span FGP with SS boundary conditions. (b) Distribution of shear stress of a 3-span FGP with SF boundary conditions. (c) Distribution of shear stress of a 3-span FGP with FF boundary conditions. (d) Distribution of shear stress of a 3-span FGP with CS boundary conditions. (e) Distribution of shear stress of a 3-span FGP with CC boundary conditions. (f) Distribution of shear stress of a 3-span FGP with CF boundary conditions.

7. Conclusion

The novel plate theory proposed by Soldatos and Watson (1997a) is extended in this paper to study the static behavior in single- and multi-span FGPs subjected to cylindrical bending with arbitrary boundary conditions. A transfer matrix method is employed to determine the shape function and it is very efficient because the order of the set of equations to be solved ultimately remains unaltered even if the number of divided layers increases for the sake of higher accuracy. The governing equations of Soldatos plate theory are also solved by the transfer matrix method, which deals excellently with arbitrary boundary conditions. In addition to the study of Soldatos and Watson (1997a,b) and Soldatos and Liu (2001), a new example, i.e. a two-layered plate in cylindrical bending subjected to various boundary conditions, is considered in this paper and comparison with the elasticity solution (Vel and Batra, 2001) does validates the present theory.

The analysis has been extended to analyze multi-span FGPs. Comparison of the present solution with the exact elasticity solution shows the Soldatos plate theory usually yields more accurate stresses than the first- and third-order shear deformation plate theories when analyzing inhomogeneous plates or plates with a high length-to-thickness ratio.

Numerical examples show that stresses in FGPs vary smoothly through the thickness, thus preventing failures due to interfacial debonding or stress concentration commonly occurs in conventional laminated materials. Moreover, FGMs are more designable. For example, Fig. 15 shows that the position of stress peak can be chosen by taking a proper value of κ. Such features endows FGPs a bright future application in electron, chemistry, optics, biomedicine, etc. The paper also extends the method to investigate multi-span plates and new numerical solutions have been obtained and discussed.

In this paper, only a one-dimensional problem is considered, i.e. plates in cylindrical bending. However, when incorporated with other methods, the present method can be extended to analyze two-dimensional plate problems. For example, for a rectangular plate with a pair of opposite edges simply supported, we can first expand the mechanical qualities in terms of Fourier series in the direction perpendicular to the simply supported edges. Then, for the reduced governing equations, we can employ the Transfer Matrix Method. Xiang et al. (2002a,b) have presented such an analysis of isotropic plates based on the classical plate theory and Mindlin plate theory.

Acknowledgments

This work was supported by the Natural Science Foundation of China (no. 10432030) and the Strategic Research Grant (SRG), City University of Hong Kong (no. 7001534).

Appendix A

The matrixes **D** and **Z** in Eq. (18) are defined as

$$\mathbf{D}=\begin{bmatrix} 0 & 0 & 0 & 0 & 0 & 1 & 0 & 0 \\ 0 & 0 & 0 & 0 & 1 & 0 & 0 & 0 \\ 0 & 0 & 0 & 0 & 0 & 0 & 1 & 0 \\ 0 & 1 & 0 & 0 & 0 & 0 & 0 & 0 \\ C_{11} & 0 & C_{12} & -C_{13} & 0 & 0 & 0 & 0 \\ 0 & 0 & 0 & 0 & 0 & 0 & 0 & 1 \\ C_{12} & 0 & C_{22} & -C_{23} & 0 & 0 & 0 & 0 \\ C_{13} & 0 & C_{23} & C_{33} & 0 & 0 & 0 & 0 \end{bmatrix}, \quad \mathbf{Z}=\begin{bmatrix} 0 & 0 & 0 & 0 & 0 & 0 & 0 & 0 \\ 0 & 0 & 0 & 0 & 0 & 0 & 0 & 0 \\ 0 & 0 & C_{00} & 0 & 0 & 0 & 0 & 0 \\ 0 & 0 & 0 & 1 & 0 & 0 & 0 & 0 \\ 0 & 0 & 0 & 0 & 1 & 0 & 0 & 0 \\ 0 & 0 & 0 & 0 & 0 & 1 & 0 & 0 \\ 0 & 0 & 0 & 0 & 0 & 0 & 1 & 0 \\ 0 & 0 & 0 & 0 & 0 & 0 & 0 & 1 \end{bmatrix} \tag{A1}$$

where

$$C_{11}=\int_{-0.5}^{0.5}\alpha_1\,\mathrm{d}\zeta,\quad C_{12}=\int_{-0.5}^{0.5}\alpha_1\bar{\varphi}_x\,\mathrm{d}\zeta,\quad C_{13}=\int_{-0.5}^{0.5}\alpha_1\zeta\,\mathrm{d}\zeta$$
$$C_{22}=\int_{-0.5}^{0.5}\alpha_1\bar{\varphi}_x^2\,\mathrm{d}\zeta,\quad C_{23}=\int_{-0.5}^{0.5}\alpha_1\bar{\varphi}_x\zeta\,\mathrm{d}\zeta,\quad C_{33}=-\int_{-0.5}^{0.5}\alpha_1\zeta^2\,\mathrm{d}\zeta \tag{A2}$$
$$C_{00}=\int_{-0.5}^{0.5}\alpha_3\left(\frac{\mathrm{d}\bar{\varphi}_x}{\mathrm{d}\zeta}\right)^2 d\zeta$$

The matrix $\widetilde{\mathbf{L}}$ and vector $\widetilde{\mathbf{R}}$ in Eq. (23) are defined as

$$\widetilde{\mathbf{L}}=\overline{\mathbf{L}}-\overline{\mathbf{L}}_{c6}\mathbf{L}_{r2}/L_{26},\quad \widetilde{\mathbf{R}}=\overline{\mathbf{R}}-(R_2/L_{26})\overline{\mathbf{L}}_{c6} \tag{A3}$$

where $\overline{\mathbf{L}}$ is an 8×8 matrix by setting zero the elements on the sixth row of the matrix $\mathbf{L}$, $\overline{\mathbf{R}}$ and $\overline{\mathbf{L}}_{c6}$ are 8×1 columns by setting zero the sixth element of $\mathbf{R}$ and $\mathbf{L}_{c6}$, respectively.

Appendix B

It is well-known that there exists an exact elasticity solution of a simply supported orthotropic plate in cylindrical bending (Pagano, 1969). It can be used as a benchmark solution for clarifying any two-dimensional simplified theory or numerical method. The basic elasticity equations can be readily converted into state space formulations in a routine way (Bahar, 1975; Fan, 1996; Chen and Lee, 2004). The state vector is composed of two displacements and two stress components and it can be expanded as:

$$\begin{Bmatrix}\overline{U}\\ \overline{W}\\ \overline{\sigma}_{zx}\\ \overline{\sigma}_{zz}\end{Bmatrix}=\frac{q_1}{c_{44}^b}\begin{Bmatrix}u_0(\zeta)\cos(\beta\xi)\\ w_0(\zeta)\sin(\beta\xi)\\ \tau_0(\zeta)\cos(\beta\xi)\\ \sigma_0(\zeta)\sin(\beta\xi)\end{Bmatrix} \tag{B1}$$

Then the state-space equation is

$$\frac{\mathrm{d}}{\mathrm{d}\zeta}\begin{Bmatrix}u_0\\ w_0\\ \tau_0\\ \sigma_0\end{Bmatrix}=\begin{bmatrix}0 & -\beta & \frac{1}{\bar{c}_{66}} & 0\\ \frac{\bar{c}_{13}}{\bar{c}_{33}}\beta & 0 & 0 & \frac{1}{\bar{c}_{33}}\\ \alpha_1\beta^2 & 0 & 0 & -\frac{\bar{c}_{13}}{\bar{c}_{33}}\beta\\ 0 & 0 & \beta & 0\end{bmatrix}\begin{Bmatrix}u_0\\ w_0\\ \tau_0\\ \sigma_0\end{Bmatrix} \tag{B2}$$

and the other two stress components are determined by

$$\begin{Bmatrix}\bar{\sigma}_{xx}\\ \bar{\sigma}_{yy}\end{Bmatrix}=\frac{q_1}{c_{44}^b}\begin{Bmatrix}-\beta\alpha_1 u_0+\frac{\bar{c}_{13}}{\bar{c}_{33}}\sigma_0\\ -\beta\alpha_2 u_0+\frac{\bar{c}_{23}}{\bar{c}_{33}}\sigma_0\end{Bmatrix}\sin(\beta\xi) \tag{B3}$$

By virtue of the continuity conditions of state variables at each fictitious interface in a laminated model as well as the boundary conditions on the top and bottom surfaces, the state vector can be determined. More details can be found in Bahar (1975), Fan (1996), Chen et al. (2004b), and Chen and Lee (2004) for examples.

References

Aboudi, J., Pindera, M., Arnold, S.M., 1995. Coupled higher-order theory for functionally grade composites with partial homogenization. Composite Engineering 5, 771–792.

Bahar, L.Y., 1975. A state space approach to elasticity. Journal of the Franklin Institute 299, 33–41.

Chen, W.Q., Ding, H.J., 2000. Bending of functionally graded piezoelectric rectangular plates. Acta Mechanica Solida Sinica 13, 312–319.

Chen, W.Q., Lee, K.Y., 2004. Three-dimensional exact analysis of angle-ply laminates in cylindrical bending with interfacial damage via state-space method. Composite Structures 64, 275–283.

Chen, W.Q., Ye, G.R., Cai, J.B., 2002. Thermoelastic stresses in a uniformly heated functionally graded isotropic hollow cylinder. Journal of Zhejiang University (Science) 3, 1–5.

Chen, W.Q., Bian, Z.G., Ding, H.J., 2003. Three-dimensional analysis of a thick FGM rectangular plate in thermal environment. Journal of Zhejiang University (Science) 4, 1–7.

Chen, W.Q., Bian, Z.G., Ding, H.J., 2004a. Three-dimensional vibration analysis of fluid-filled orthotropic FGM cylindrical shells. International Journal of Mechanical Sciences 46, 159–171.

Chen, W.Q., Bian, Z.G., Lv, C.F., Ding, H.J., 2004b. 3D free vibration analysis of a functionally graded piezoelectric hollow cylinder filled with compressible fluid. International Journal of Solids and Structures 41, 947–964.

Cheng, Z.Q., Batra, R.C., 2000. Exact correspondence between eigenvalues of membranes and functionally graded simply supported polygonal plates. Journal of Sound and Vibration 229, 879–895.

Cheung, Y.K., Zhou, D., 2000. Vibrations of rectangular plates with elastic intermediate line-supports and edge constraints. Thin-Walled Structures 37, 305–331.

Croce, L.D., Venini, P., 2004. Finite elements for functionally graded Reissner–Mindlin plates. Computer Methods in Applied Mechanics and Engineering 193, 705–725.

Delale, F., Erdogan, F., 1988. On the mechanical modeling of the interfacial region in bonded half-planes. Journal of Applied Mechanics 55, 317–324.

Fan, J.R., 1996. Exact Theory of Strongly Thick Laminated Plates and Shells. Science Press, Beijing (in Chinese).

Folds, D.L., Loggins, C.D., 1977. Transmission and refection of ultrasonic waves in layered media. Journal of the Acoustical Society of America 62, 1102–1109.

Fuchiyama, T., Noda, N., 1995. Analysis of thermal stress in a plate of functionally gradient material. JSAE Review 16, 263–268.

Haskell, N.A., 1953. The dispersion of surface waves in multilayered media. Bulletin of the Seismological Society of America 43, 17–34.

Khdeir, A.A., 1996. A remark on the state-space concept applied to bending, buckling and free vibration of composite laminates. Computers and Structures 59, 813–817.

Koizumi, M., 1997. FGM activities in Japan. Composites B 28, 1–4.

Kong, J., Cheung, Y.K., 1995. Vibration of shear-deformable plates with intermediate line supports: A finite layer approach. Journal of Sound and Vibration 184, 639–649.

Lam, K.Y., Li, H., 1997. Vibration analysis of a rotating truncated circular conical shell. International Journal of Solids and Structures 34, 2183–2197.

Li, C.Y., Weng, G.J., 2002. Antiplane crack problem in functionally graded piezoelectric materials. Journal of Applied Mechanics 69, 481–488.

Li, H., Lam, K.Y., 2001. Orthotropic influence on frequency characteristics of a rotating composite laminated conical shell by the generalized differential quadrature method. International Journal of Solids and Structures 38, 3995–4015.

Li, Q.S., 2003. An exact approach for free vibration analysis of rectangular plates with line-concentrated mass and elastic line-support. International Journal of Mechanical Sciences 45, 669–685.

Liew, K.M., He, X.Q., Ray, T., 2004. On the use of computational intelligence in the optimal shape control of functionally graded smart plates. Computer Methods in Applied Mechanics and Engineering 193, 4475–4492.

Liu, G.R., Han, X., Lam, K.Y., 1999. Stress waves in functionally gradient materials and its use for material characterization. Composites Part B: Engineering 30, 383–394.

Liu, G.R., Dai, K.Y., Han, X., Ohyoshi, T., 2003. Dispersion of waves and characteristic wave surfaces in functionally graded piezoelectric plates. Journal of Sound and Vibration 268, 131–147.

Ma, L.S., Wang, T.J., 2004. Relationships between axisymmetric bending and buckling solutions of FGM circular plates based on third-order plate theory and classical plate theory. International Journal of Solids and Structures 41, 85–101.

Munjal, M.L., 1975. Velocity ratio cum transfer matrix method for the evaluation of a muffler with mean flow. Journal of Sound and Vibration 39, 105–119.

Munjal, M.L., 1993. Response of a multilayered infinite plate to an oblique plane wave by means of transfer matrices. Journal of Sound and Vibration 162, 333–344.

Nayfeh, A.N., 1991. The general problem of elastic wave propagation in multilayered anisotropic media. Journal of the Acoustical Society of America 89 (Part I), 1521–1531.

Pagano, N.J., 1969. Exact solutions for composite laminates in cylindrical bending. Journal of Composite Materials 3, 398–411.
Pestel, E.C., Leckie, F.A., 1963. Matrix Methods in Elastomechanics. McGraw-Hill, New York.
Praveen, G.N., Reddy, J.N., 1998. Nonlinear transient thermal elastic analysis of functionally graded ceramic-metal plates. International Journal of Solids and Structures 35, 4457–4476.
Qian, L.F., Batra, R.C., Chen, L.M., 2004. Static and dynamic deformations of thick functionally graded elastic plates by using higher-order shear and normal deformable plate theory and meshless local Petrov–Galerkin method. Composites: Part B 35, 685–697.
Rabin, B.H., Shiota, I., 1995. Functionally gradient materials. Materials Research Society Bulletin 20, 14–18.
Reddy, J.N., 2000. Analysis of functionally graded plates. International Journal for Numerical Methods in Engineering 47, 663–684.
Reddy, J.N., Wang, C.M., Kitipornchai, S., 1999. Axisymmetric bending of functionally graded circular and annular plates. European Journal of Mechanics A/Solids 18, 185–199.
Stepanishen, P.R., Strozeski, B., 1982. Reflection and transmission of wideband plane acoustic waves by layered viscoelastic media. Journal of the Acoustical Society of America 71, 9–21.
Soldatos, K.P., Liu, S.L., 2001. On the generalised plane strain deformations of thick anisotropic composite laminated plates. International Journal of Solids and Structures 38, 479–482.
Soldatos, K.P., Watson, P., 1997a. A method for improving the stress analysis performance of one- and two-dimensional theories for laminated composites. Acta Mechanica 123, 163–186.
Soldatos, K.P., Watson, P., 1997b. Accurate stress analysis of laminated plates combining a two-dimensional theory with the exact three-dimensional solution for simply supported edges. Mathematics and Mechanics of Solids 2, 459–489.
Thomson, W.T., 1950. Transmission of elastic waves through a stratified solid medium. Journal of Applied Physics 21, 89–93.
Vel, S.S., Batra, R.C., 2000. The generalized plane strain deformations of thick anisotropic composite laminated plates. International Journal of Solids and Structures 37, 715–733.
Vel, S.S., Batra, R.C., 2001. Closure to the generalized plane strain deformations of thick anisotropic composite laminated plates. International Journal of Solids and Structures 38, 483–489.
Wu, C.C.M., Kahn, M., Moy, W., 1996. Piezoelectric ceramics with functional gradients: A new application in material design. Journal of American Ceramic Society 79, 809–812.
Wu, L.H., 2004. Thermal buckling of a simply supported moderately thick rectangular FGM plate. Composite Structures 64, 211–218.
Xiang, Y., Zhao, Y.B., Wei, G.W., 2002a. Exact solutions for vibration of multi-span rectangular Mindlin plates. Journal of Vibration and Acoustics 124, 545–551.
Xiang, Y., Zhao, Y.B., Wei, G.W., 2002b. Levy solutions for vibration of multi-span rectangular plates. International Journal of Mechanical Sciences 44, 1195–1218.
Zhou, D., 1994. Eigenfrequencies of line supported rectangular plates. International Journal of Solids and Structures 31, 347–358.